Nuclear Science and Technology Division (94)

Monte Carlo Modeling of a Fork Detector System

B. D. Murphy* and P. De Baere**

* Oak Ridge National Laboratory, Oak Ridge, Tennessee 37831-6170, U.S.A.
** European Commission, DG TREN I1-2 Luxembourg

E-mail: murphybd@ornl.gov, Paul.DE-BAERE@cec.eu.int

Presented at the
27th Annual Meeting
Symposium on Safeguards and Nuclear Material Management
May 10–12, 2005,
London, England

The submitted manuscript has been authored by a contractor of the U.S. Government under contract No. DE-AC05-00OR22725. Accordingly, the U.S. Government retains a nonexclusive, royalty-free license to publish or reproduce the published form of this contribution, or allow others to do so, for U.S. Government purposes.

Monte Carlo Modeling of a Fork Detector System

B. D. Murphy* and P. De Baere**

* Oak Ridge National Laboratory, Oak Ridge, Tennessee 37831-6170, U.S.A.[a]
** European Commission, DG TREN I1-2 Luxembourg
E-mail: murphybd@ornl.gov, Paul.DE-BAERE@cec.eu.int, gauldi@ornl.gov

Abstract:

Monte Carlo simulations are described for the response of a Fork detector system used to estimate neutron and gamma count rates from a spent-fuel assembly. Using spent-fuel source-strength characterizations from the Oak Ridge National Laboratory (ORNL) Standardized Computer Analyses for Licensing Evaluation (SCALE) system and the Monte Carlo Neutron-Particle (MCNP) code, Fork detector responses were estimated by starting with the fuel characterization and burnup history of an assembly. Detector response to neutrons and photons is described for pressurized-water-reactor (PWR) and boiling-water-reactor (BWR) systems. Particle fluxes are calculated, and detector signals are then estimated. Some preliminary benchmarking is discussed using Fork measurement data from a small number of spent-fuel assemblies.

Keywords: Monte Carlo; Fork detectors; spent fuel

1. Introduction

Fork radiation detectors[1] are commonly used to monitor spent-nuclear-fuel assemblies. They provide a convenient nondestructive means for characterizing fuel assemblies following discharge. These Fork detectors are physically located outside the assembly and provide information on the neutron and gamma radiation fields emanating from the spent fuel. In safeguards applications, it is of interest to determine if such a system can detect anomalies in spent-fuel assemblies (e.g., missing fuel rods); another application of the Fork detector would be the verification of assembly burnup. The response of a Fork detector is complicated, and the interpretation of detector response for a particular assembly configuration requires careful analysis.

ORNL maintains and develops the ORNL SCALE[2] system with many applications to reactor analysis and related areas. One prominent application of SCALE is for the analysis of fuel-assembly burnup and the determination of the characteristics of spent fuel. In an effort to proceed from the characterization of spent fuel to the determination of Fork detector response, we developed a Monte Carlo transport model to simulate detector response by starting with the spent-fuel-assembly source composition. This Monte Carlo approach is based on the MCNP code[3]. In this paper we describe the MCNP model leading to the determination of Fork detector response. The ORNL SCALE system is used to determine the MCNP source strengths that drive the transport calculations. We also discuss preliminary benchmarking studies that compare calculated results against neutron and gamma measurements performed by the European Atomic Energy Community (EURATOM).

2. MCNP models of detectors and assemblies

The MCNP model discussed here consists of a Fork detector plus a spent-fuel assembly. Currently, the model exists in two versions, which treat BWR and PWR fuel assemblies. The MCNP model includes the assembly (BWR or PWR with fuel rods and water rods, as the case may be) and two Fork

[a] Managed by UT-Battelle, LLC, for the U.S. Department of Energy under contract No. DE-AC05-00OR22725

detector arms mounted such that one is on each side of the assembly. Generally, because measurements are performed in the cooling pool, this entire system is immersed in water. The cooling-pool water may also contain boron. For the PWR cases studied, the model has 2200 ppm of boron in the water. In the BWR cases, the water was boron free. These particular boron concentration values were chosen because they apply to the cases used for benchmarking. The data on Fork detector design and performance that are used here, as well as the data used for benchmarking, were obtained from EURATOM[4].

The example used for the PWR case involves a Westinghouse 17 × 17 PWR fuel assembly containing 264 fuel rods. The BWR case contains an 8 × 8 assembly. The 8 × 8 assembly has 1 water rod and 63 fuel rods. The material composition of the fuel rods was that of fuel irradiated to 40 GWd/t. However, it contained just the actinide component; fission products were not included.

Each arm of the Fork detector contains two fission chambers for neutron detection and an ionization chamber for gamma detection. One of the fission chambers is surrounded by high-density polyethylene (HDPE), which is covered with a 0.5 -mm cadmium shield. The other fission chamber is uncovered, although it is inside a 4-mm-thick cylindrical shell of HDPE that surrounds all of the detectors. The cadmium reduces the thermal neutron flux from the pool, and the HDPE then thermalizes the faster neutrons that penetrate the cadmium. In the descriptions that follow, the chamber to the inside of the cadmium shield will be referred to as the shielded chamber and the other chamber will be referred to as the unshielded chamber. The ionization chamber is encased in a cylindrical brass tube with a 2-mm wall thickness and is surrounded by the HDPE and cadmium layers.

The Fork detector arms are placed on each side of the assembly with the assembly located midway between them. Because of the different widths of BWR and PWR assemblies, the separation distance between the arms is different in the two cases. The inside distances between the arms are 16.8 and 24.3 cm in the BWR and PWR cases, respectively. Figure 1 is a vertical cross section showing the two detector arms with an 8 × 8 assembly located between them. Two fission chambers and one ionization chamber (surrounded by a brass sleeve) can be seen in each arm. The detector arms are the same but are rotated by 180 degrees relative to one another. Fork detector arms have a diameter of 9.2 cm.

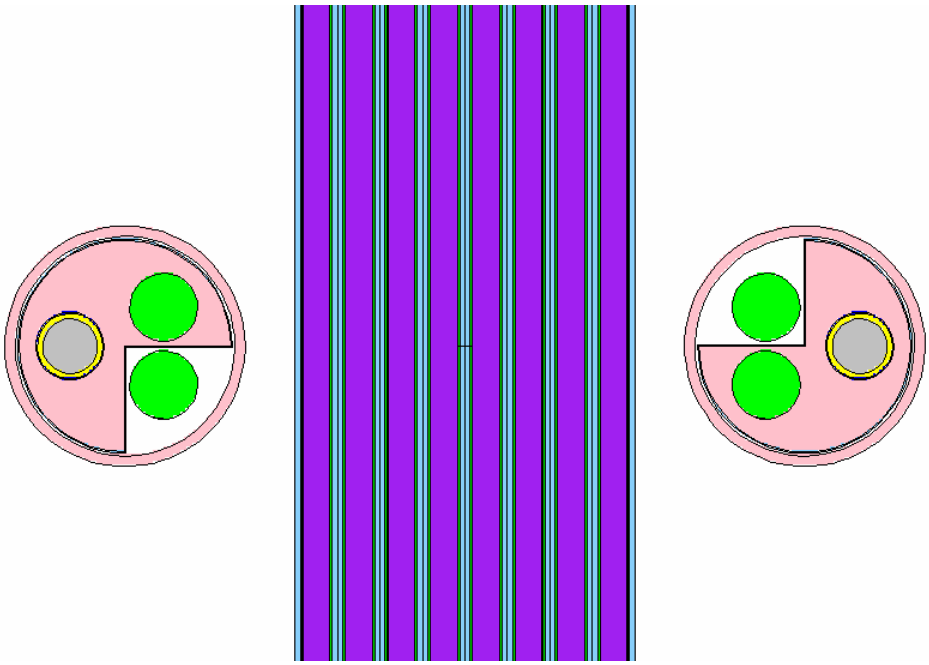

Figure 1. Vertical cross section through the Fork detector arms with an 8 × 8 BWR assembly. For the arm on the right of the figure, the two fission chambers are to the left, with the bottom one shielded and the top one unshielded. The ionization chamber is to the right. Both arms are the same but are rotated by 180 degrees around the horizontal axis relative to one another.

3. Detector response estimation

MCNP calculations result in particle flux estimates. The fluxes are calculated as a function of energy. The gamma detector (an ionization chamber) has a response that is a function of exposure. If one determines the photon flux as a function of energy, one can then determine exposure via a conversion factor that is a function of energy. The fission chambers register counts that correspond to fission events occurring in the wall coating which is enriched in ^{235}U. Fission chambers are mostly sensitive to thermal neutrons; however, for accurate calculation of the total response, one needs to determine neutron flux as a function of energy and then use the energy-dependent fission cross section to determine fission rates in the chamber.

The radiation sources are modeled within each spent-fuel rod, with the total source strength determined using the concentration of the various nuclide species in the fuel at the measurement time of interest (e.g., ^{137}Cs, an important gamma emitter, and ^{244}Cm, an important source of neutrons). Source strength, in general, may vary as a function of position within the assembly. MCNP is capable of defining complicated source configurations; axial and horizontal variations in source strength can easily be accommodated. MCNP also allows flexibility in the specification of the source-energy spectrum. Source-energy spectra are output from SCALE codes that simulate assembly burnup and cooling. Energy-bin boundaries can be determined by the user, and MCNP can accept any arbitrary set of bin boundaries.

4. Preliminary efficiency and normalization studies

In the initial simulation runs, overall efficiencies of the 17×17 and 8×8 models were assessed. As might be expected, for a given number of histories, the 8×8 case executes more quickly. (There are fewer cells and the geometry is simpler, giving rise to less complicated trajectories.) Neutron-tracking cases take considerably longer than photon-tracking cases. From early test results, it is also apparent (especially for gamma sources) that the internal fuel rods make negligible contributions to the detector counts. So, for purposes of efficiency one may apply biasing techniques to lower the importance of the internal rods.

There is one gamma-counting device (an ionization chamber) in each arm of the Fork detector and, for neutron detection, there is one shielded and one unshielded fission chamber in each arm. The ionization chamber produces a signal that is proportional to dose rate. The Fork detector ionization chambers are quoted by the manufacturer as having a response of 3.4×10^{-10} A/R/h. Because the transport calculations result in estimates of photon flux, it is necessary to convert calculated photon fluxes to dose rates using flux-to-dose-rate conversion factors. Then, via the response function of the ionization chamber, the magnitude of the ionization chamber gamma signal can be determined. The flux-to-dose-rate conversion factors are functions of energy, and the photon flux tallies from MCNP are scored in energy bins.

The fission chambers in the Fork detector have a thin layer of UO_2 on the inside cylindrical surface. This layer is enriched to 93% in ^{235}U so that an effective surface density of 850 μg/cm^2 exists for ^{235}U. The quoted detector response is 0.14 cps/nv, which is to be interpreted as counts per second per unit of flux. (We assume this value applies to thermal neutrons.) Figure 2 shows the results of an MCNP simulation for a layer of UO_2 with the design concentration of ^{235}U on the inside of one of the fission chambers. The fission rate can be seen to reproduce the quoted chamber response value for thermal neutrons. (Presumably, the chamber response does not account for self-absorption of fission fragments.) In determining the response of a neutron detector, the energy-dependent neutron flux, together with the energy-dependent fission cross section, is used to estimate the fission rate in the UO_2 on the inside of the chamber wall.

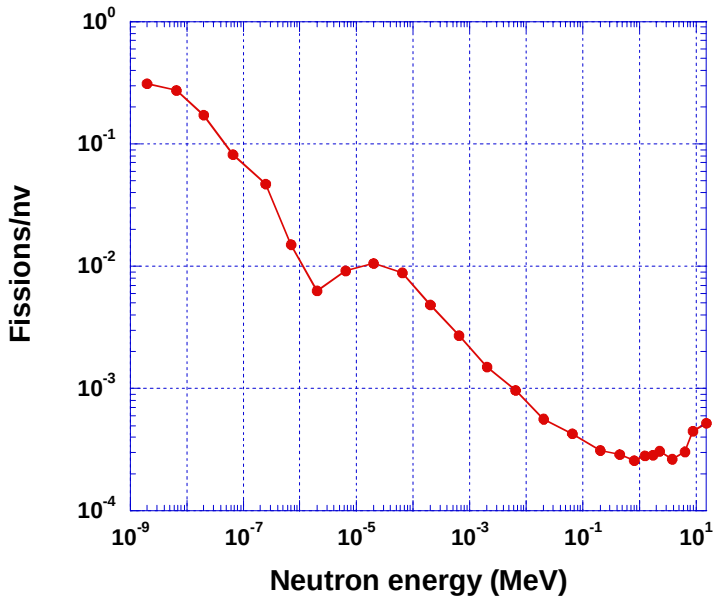

Figure 2. Fission rate versus neutron energy for the fission chamber. This has the form of the ^{235}U fission cross section and reproduces the quoted response of 0.14 cps/nv at 0.025 eV.

5. Neutron and gamma response functions

Fork detector responses to neutrons and photons have been estimated as a function of the originating neutron or photon energy. This was done for both a 17 × 17 PWR and an 8 × 8 BWR. We will later refer to an 18 × 18 PWR case and a 9 × 9 BWR case when discussing benchmarking studies. The response in the 9 × 9 case is similar to that of the 8 × 8, and the 17 × 17 can be considered as representative of an 18 × 18. The various calculated results will be presented versus the energy of the originating neutron or photon. These results are per neutron or photon for the average neutron or photon originating in the assembly. The calculations assume that the radiation source within the assembly is distributed among the fuel rods in a horizontally uniform manner. However, the source strength has an axial profile, which is a typical assembly axial profile. All measurements and simulations will be for the assembly centerline.

Spent-fuel composition and the source strength are independently specified in the MCNP model. The spent-fuel composition is intended to be representative of a discharged assembly. Because all significant actinides are included in the composition, the Monte Carlo calculations account for secondary fission neutrons. However, the fuel assembly model did not contain neutron poisons.

6. Neutron response results

Neutron results are presented both as neutron flux at the location of the two fission chambers (the shielded and unshielded chambers) and as count rates in these detectors. Because of the symmetrical arrangement of the Fork detector arms, the response in a particular type of detector will be the same for both arms of the detector (within the statistical limits of the stochastic Monte Carlo process). Most results reported here were obtained by calculating an average for the two detector arms; but all quoted values are per detector. The flux values (neutrons/cm^2/s) are averages for the region occupied by the active part of the fission chamber. The count rates are determined from the

flux, the ^{235}U fission cross section, the ^{235}U density, and the volume of the UO_2 layer that coats the inside surface of the fission-chamber wall. The reaction rate, *R*, is calculated using the thin-target approximation, as in

$$R = Nn\sigma d$$

where *N* is the number of incident particles/s, *n* is the density of ^{235}U nuclei, and *d* is the thickness of the UO_2 layer. Note that the fission rates are calculated from the average flux in the region occupied by the UO_2 layer, whereas the flux values that are quoted are averages over the full active volume of the fission chamber. However, the flux in both regions is essentially the same.

In the figures that follow, neutron fluxes are presented both as total flux and as flux below 0.4 eV. The flux below 0.4 eV will be referred to as the thermal flux (the flux below the cadmium cutoff). The flux values (total and thermal) and the count rates are presented as functions of the energy of the neutron originating in the assembly. Figures 3–6 show various neutron simulation results. Total flux per originating neutron in the 17×17 assembly is shown in Figure 3. Results are shown for both the shielded and unshielded fission chambers. Figure 4 shows total flux from the 8×8 assembly. The 8×8 values are higher, probably reflecting the fact that the average neutron originating in that assembly is nearer to the detector than is the case for the 17×17 assembly. (Note also the different relative spacing of the shielded and unshielded values in the PWR and BWR cases; see below for more discussion of this.) These neutron fluxes produce counts in the fission chambers. Figure 5 shows the resulting count rates in both the shielded and unshielded fission chambers for the 8×8 BWR case (per originating neutron). The fission chamber is mostly responsive to thermal neutrons, as seen in the thermal neutron flux (flux below 0.4 eV) for the 8×8 case shown in Figure 6. By comparison of Figures 5 and 6, one can see that the fission-chamber signal is driven by the thermal flux. For the chamber count-rate curves, we show least-squares fits, whereas for the flux plots, the calculated points are simply connected with straight lines. In general, the scatter seen in the calculated points results from the stochastic nature of the Monte Carlo calculations. It should, however, be noted that a real depression in flux, caused by a resonance in ^{16}O, is seen around 5 MeV.

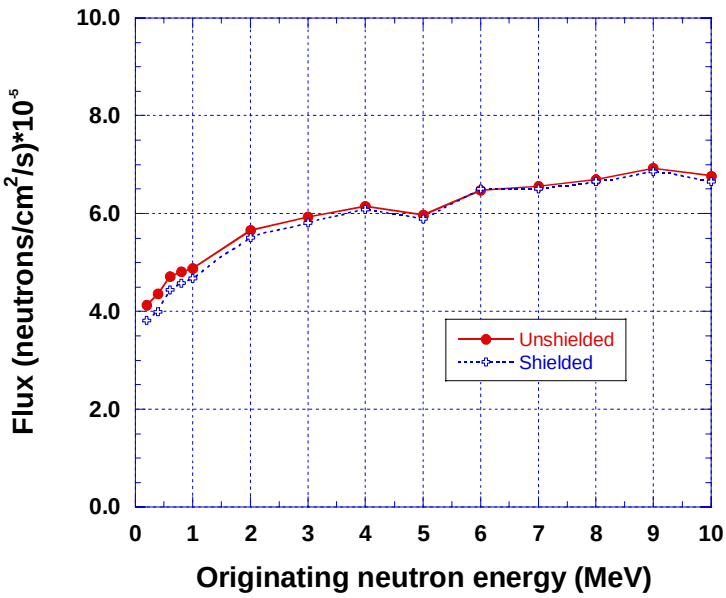

Figure 3. Total neutron flux (i.e., per originating assembly neutron per second) at the fission chambers as a function of originating neutron energy for a 17×17 PWR assembly. The calculated values have been joined by straight lines. Although there is some statistical scatter in the results, the depression around 5 MeV is real and is caused by a resonance in ^{16}O.

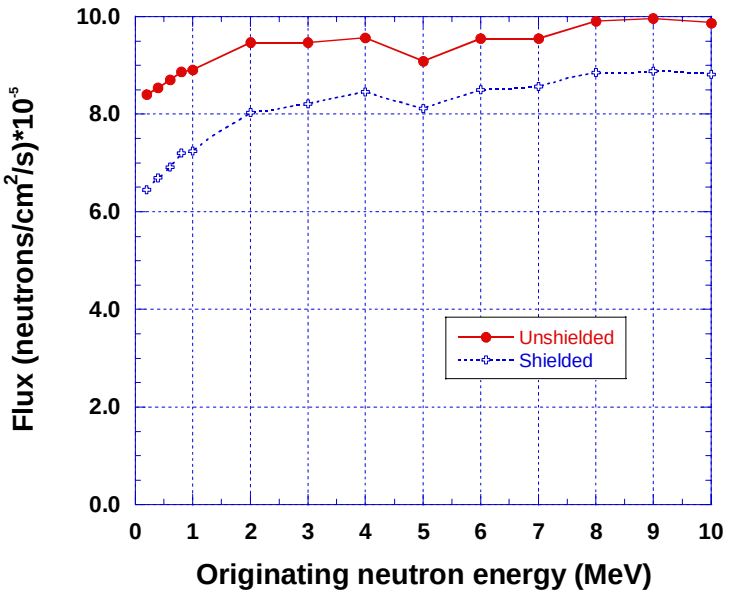

Figure 4. Total neutron flux (i.e., per originating assembly neutron per second) at the fission chamber versus neutron energy for the 8 × 8 BWR assembly. Again, note the flux depression around 5 MeV.

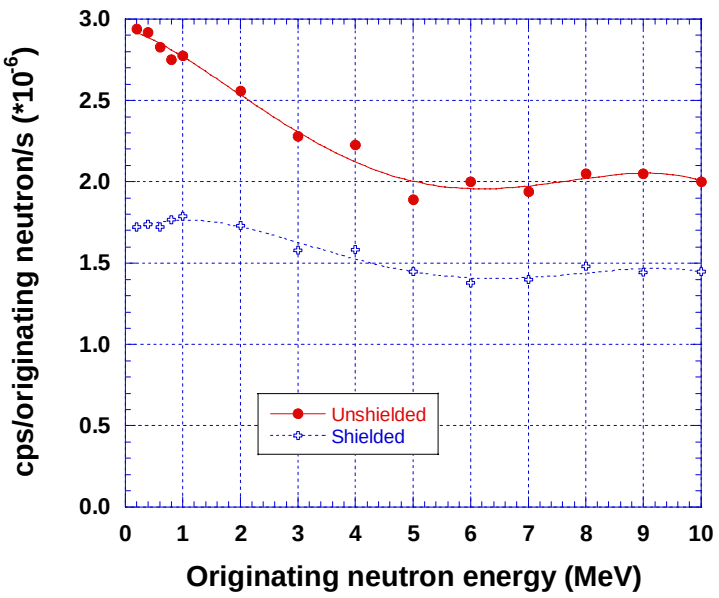

Figure 5. Fission-chamber count-rate response for the 8 × 8 BWR case. The points are the calculated values. They include statistical scatter and have been fitted with smooth curves.

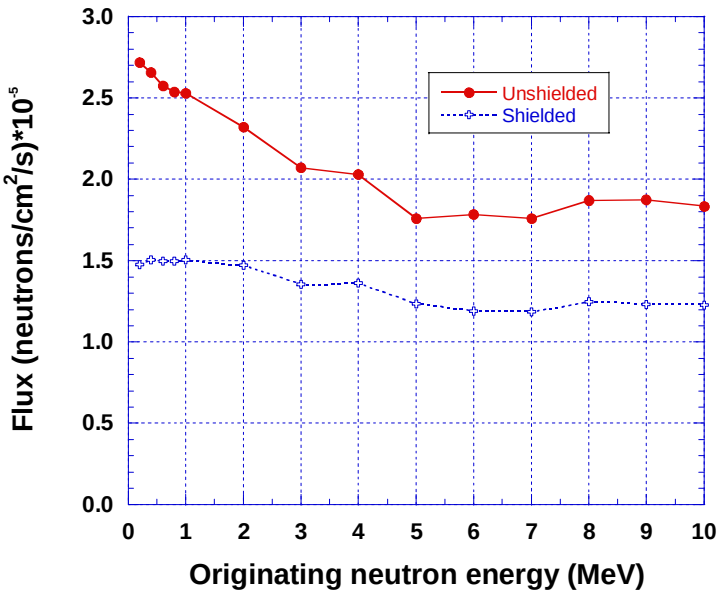

Figure 6. The thermal (< 0.4 eV) neutron flux at the fission chambers for the 8 × 8 BWR case.

Figure 7 shows the fission-chamber count-rate response (shielded and unshielded) in the case of the 17 × 17 Fork configuration. This figure should be compared with Figure 5. As was noted, it is mostly thermal neutrons that contribute to the fission-chamber response. Therefore, keeping in mind that the PWR pool contains boron and the BWR pool does not, fewer thermal neutrons will reach the vicinity of the detectors in the PWR case. Consequently, the unshielded detector will see less thermal neutrons from the PWR, thus leading to a lower signal, as is evident from the figures. (This is also reflected in the unshielded flux being relatively lower in Figure 3 as compared with than in Figure 4.)

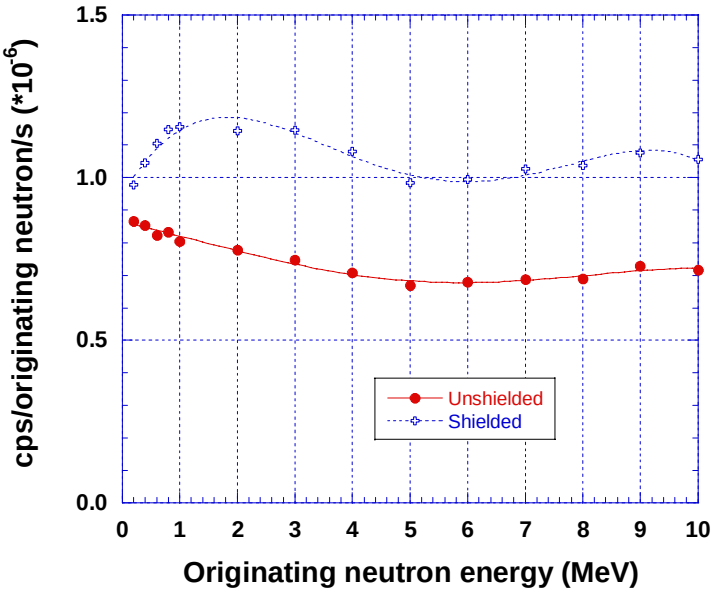

Figure 7. The fission-chamber count-rate response for the 17 × 17 PWR case. The calculated points have been fitted with smooth curves.

The shielded detectors are expected to detect fast neutrons that pass through the cadmium and are then thermalized in the HDPE. This neutron population should not be greatly influenced by the boron and therefore should be similar for the BWR and PWR cases. However, note that the average neutron originating in the PWR assembly is farther from the detectors than in the BWR case (and is subject to more shielding). So, although we expect rough agreement between shielded responses (per originating neutron) for the BWR and PWR, the PWR response should be somewhat lower. Again, this is evident from the figures.

The count-rate response curves show a fairly flat energy response, and, furthermore, the shape of the neutron energy spectrum does not vary appreciably from case to case. Therefore, it was not surprising to find that a standard form of neutron energy spectrum seemed to suffice for all calculations. Thus, we have chosen to use the ^{244}Cm neutron decay spectrum for all calculations.

Table 1 summarizes MCNP-predicted fission rates at the chamber locations when the neutron spectrum is that of a ^{244}Cm source. Specifically, the quantities in Table 1 are fissions per cubic centimeter, in the UO_2 layer, per originating neutron.

	BWR	PWR
Unshielded	2.36×10^{-4}	7.45×10^{-5}
Shielded	1.59×10^{-4}	1.032×10^{-4}

Table 1. Summary of MCNP fission rates from a ^{244}Cm source (fissions per cubic centimeter).

7. Gamma response results

The gamma results are presented in two ways. We show both the photon flux and the (hypothetical) gamma dose rate over the active part of the ionization chamber. Again, the results reported are per originating photon and are shown as a function of the originating photon energy. The primary quantity that is calculated is the photon flux versus energy at the chamber location. The ionization properties of the radiation field are probably best described in terms of the exposure. However, flux-to-dose-rate conversion factors are readily available and these were employed to convert the gamma flux to the dose rate. The chamber sensitivity is quoted in terms of dose, and the resulting signal can then be calculated.

The photon flux for the 8×8 case is illustrated in Figure 8. This is the total flux at the ionization chamber per originating photon per second. The shape of the curve shows that low-energy photons are less likely to escape from the assembly, because of photoelectric capture in the high-Z fuel material. The resulting photon dose is shown in Figure 9. Results from two separate dose-rate-response functions are shown; one set of results was obtained using American National Standards Institute/American Nuclear Society (ANSI/ANS) flux-to-dose-rate conversion factors[5], and the other set was obtained using International Commission on Radiological Protection (ICRP) conversion factors[6]. The results for the 17×17 PWR case are quite similar.

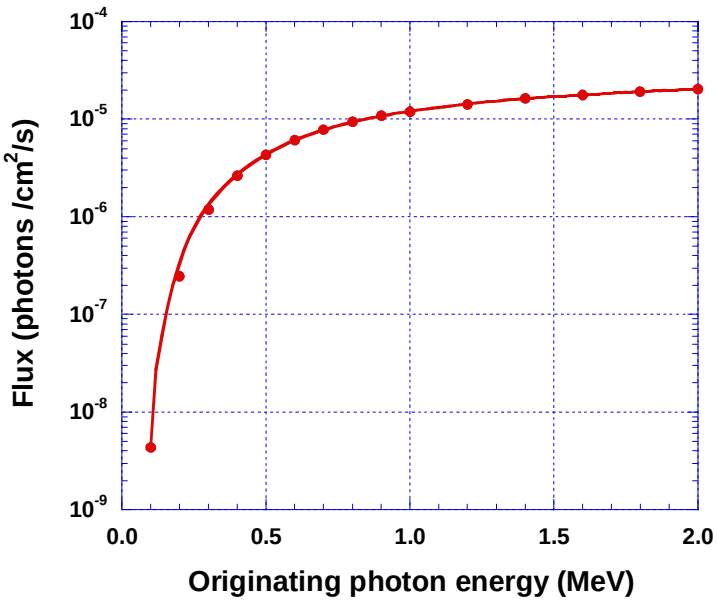

Figure 8. Photon flux (i.e., per originating photon per second) at the ionization chamber for the 8 × 8 BWR case. This is shown as a function of originating photon energy.

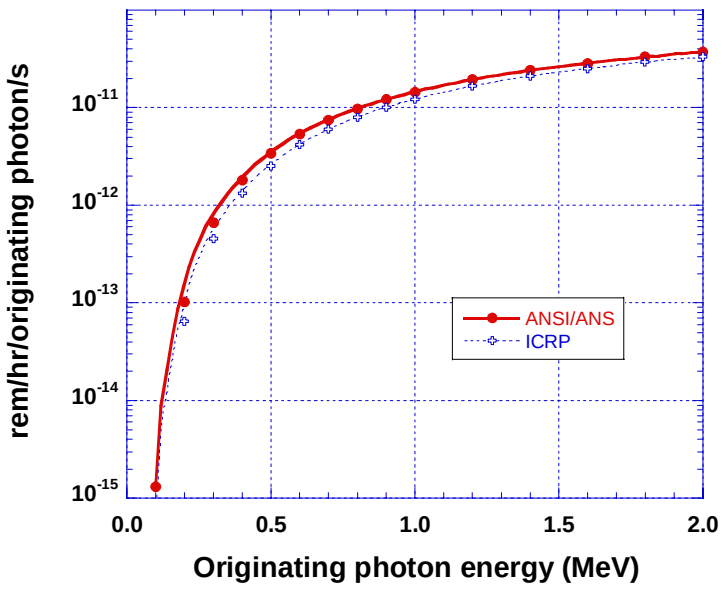

Figure 9. Photon dose results for the 8 × 8 BWR case as a function of originating photon energy. These values are dose rate (per hour) per originating photon rate (per second). Values calculated with both sets of flux-to-dose-rate conversion factors are shown.

8. Benchmarking of Fork simulations

Measurement data obtained by EURATOM were used to conduct benchmarking studies to see how well SCALE and MCNP reproduce the observed counts. Ideally, if trends versus burnup are to be readily detectable, it is desirable that all measurements be made on fuels that have the same initial enrichment and have experienced the same cooling time. In checking measurements reported for Fork detectors, one finds that most groups of measurements cover short burnup ranges (i.e., < 5,000 MWd/t). Because of scatter in the measurements, longer burnup ranges (e.g., > 10,000 MWd/t) may be needed in order to estimate trends.

Two groups of measurement data were examined. One group was for assemblies from a 9 × 9 BWR, and one was for assemblies from an 18 × 18 PWR. An 8 × 8 model and a 17 × 17 model were used to simulate the BWR and PWR assemblies, respectively, with neutron and gamma source strengths determined from the SAS2/ORIGEN-S sequences in the SCALE system. (The overall dimensions of the BWR and PWR modeled assemblies were essentially the same as the measured ones.)

9. Neutron results

Burnup for the 16 BWR assemblies studied ranged from about 29 to 32.4 GWd/t. All had an initial enrichment of approximately 2.6%. (For proprietary reasons, quoted numbers are rounded values, and the specific assemblies are not identified.) Measured data points are shown in Figure 10 for neutron counters A and B (shielded and unshielded, respectively). Calculated values are also shown for both the shielded and unshielded cases. The measured data points show scatter. Second-degree polynomial fits are shown for both sets. From Figure 10 we note that neutron A (shielded) counts are lower than the neutron B (unshielded) counts and that for the calculated values the shielded count rates are also lower than the unshielded ones. As explained, this should be the case for assemblies that do not have boron in the cooling-pool water. However, the trends as a function of burnup are not the same for measured and calculated count rates. (The measured values seem to increase more strongly with burnup.) With the amount of spread and the burnup range, one cannot be definitive about the trends in the measured data.

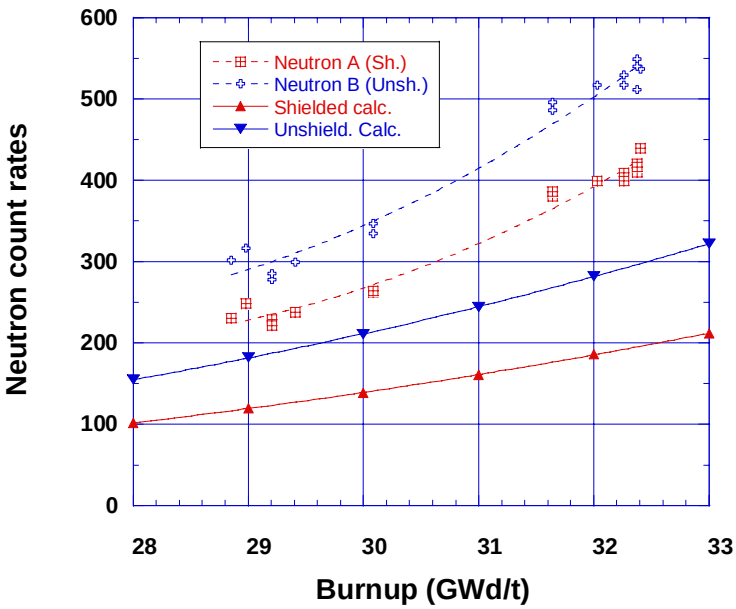

Figure 10. Neutron results for the BWR assemblies. The cooling pool does not contain boron, and unshielded rates are higher than shielded rates. Trends with burnup are different for the measured and the calculated cases. Second-degree polynomial fits are shown for the measured and calculated values.

The neutron results for the second set of assemblies (18 × 18 PWR) are shown in Figure 11. This set consists of five assemblies with initial enrichments of approximately 3.4% and with burnups ranging from about 34 to 41.6 GWd/t. Because of variations in enrichment, cooling time, and out-of-reactor time between irradiation cycles, we do not expect a smooth trend as a function of burnup. Again, estimated count rates are lower than measured ones. For these PWR assemblies there is boron in the pool water (2200 ppm) and, for both the measured and calculated points, the values for shielded count rates are higher. From Figure 11 one can see that the trend in the measured values is reproduced quite well by the simulations.

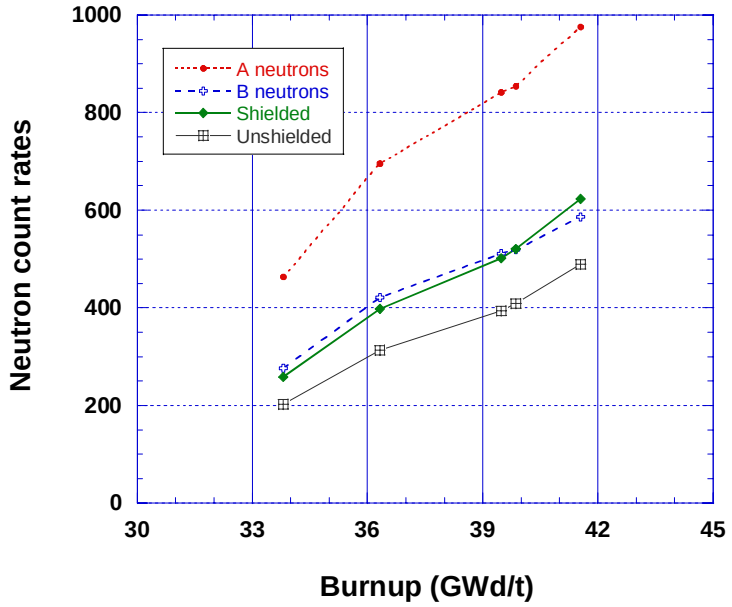

Figure 11. Neutron results for the PWR assemblies. The cooling pool contains 2200 ppm of boron, and shielded rates are higher than unshielded rates. Trends with burnup are similar for the measured and the calculated cases.

In summary, the neutron comparisons show two notable characteristics. (1) The observed count rates in the neutron detectors are higher than what are predicted. (2) Although measured and calculated trends as a function of burnup are similar in the PWR case, they are not so in the BWR case. A couple of possibilities come immediately to mind for the higher count rates: It may be that the active region of the fission chamber is larger than what was used in the simulations, or perhaps the fission chambers are affected by the gamma flux. (The gamma flux immediately outside a spent-fuel assembly can be as much as seven orders of magnitude higher than the neutron flux.) However, it is not surprising that count rates do not match exactly. We expect that in a practical application of this work, a normalization factor would be required.

One likely explanation for the lower calculated neutron count rates is that estimates of neutron source strength for the spent-fuel assemblies are low. The majority of the neutrons are from ^{244}Cm. The ^{244}Cm concentration is determined using reactor-burnup-simulation codes (from the SCALE system) and is subject to some degree of uncertainty. Work performed at ORNL[7] comparing simulations with destructive-analysis measurements indicates that ^{244}Cm concentrations seem to be underpredicted. Before addressing this possible underprediction, however, we first wish to discuss the differences in trends seen for measurements and calculations in the BWR case. This difference seems to indicate that neutron source strength in the BWR assemblies is increasing at a faster rate versus burnup than the calculations indicate. Because the neutron flux is mostly from ^{244}Cm, should there be zoning of enrichment levels among the fuel pins (with low enrichments to the outside), higher concentrations of ^{244}Cm to the outside would result. (In order to maintain uniform power, the neutron flux will increase in the low-enrichment areas, thus leading to increased actinide transmutation rates.) Thus, with enrichment zoning, neutron count rates could be higher than would be the case for assemblies with uniform enrichment and the neutron count rates would show a larger increase as a function of burnup.

Returning to the issue of ^{244}Cm underprediction, we note that the ORNL comparisons between experimentally determined concentrations and burnup simulation calculations involved both mixed-oxide (MOX) and low-enriched-uranium (LEU) fuels[7]. (Most of these investigations did not use the SCALE system, but some of the early investigations showed similar underpredictions using SCALE.) For both MOX and LEU, there was underprediction of ^{244}Cm concentrations relative to measurements. Two LEU samples were analyzed, and the results are relevant here. One LEU sample experienced a burnup of 31.2 GWd/t; for the other sample, the burnup was 52.4 GWd/t. Laboratory analysis and burnup-simulation calculations resulted in a calculated-to-experimental (C/E) ratio of 0.84 for ^{244}Cm in the first sample, with a measurement uncertainty of 3% (95% confidence level). The second sample was analyzed independently at two separate laboratories and yielded C/E ratios of 0.73 and 0.86. The experimental values for the second sample had uncertainties of 13 and 3%, respectively. On the basis of these results, it is reasonable to assume a C/E ratio of 0.85 for ^{244}Cm and to increase the neutron source-strength estimates accordingly. This would improve the agreement between calculations and measurement considerably.

10. Photon results

We have carried out photon (gamma) transport calculations for the 9 × 9 BWR assemblies; however, no gamma calculations were carried out for the PWR cases. Figure 12 shows the gamma results for the 9 × 9 BWR assemblies. The experimentally measured values are shown as well as the calculated values obtained by using ICRP flux-to-dose-rate conversion factors. The agreement between calculation and experiment is encouraging, although the predictions tend to be high. A later version of ICRP conversion factors exists and would likely lower the estimates by about 10%. The ICRP values that were used were readily available and were considered appropriately conservative for shielding studies. Again, in a practical application, a normalization factor is probably required.

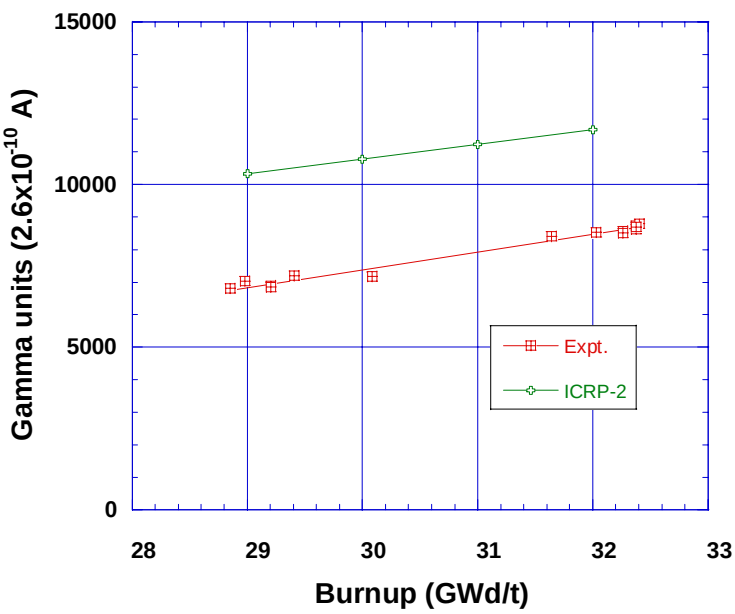

Figure 12. Gamma results for the BWR assemblies. Although the calculated values are higher, the trends are similar.

11. Summary and discussion

Monte Carlo models were developed that analyze Fork detector operation with both BWR and PWR spent-fuel assemblies. With spent-fuel characterizations obtained using the SCALE system, response functions were calculated for neutron and photon measurements and for both assembly arrangements.

Using monitoring data obtained by EURATOM, we performed benchmarking studies that compare trends between the measured data and model predictions. The results of the benchmarking studies are encouraging, but there are questions that remain to be answered.

The observed count rates in the neutron detectors are higher than what are predicted. Measured and calculated trends as a function of burnup are similar in the PWR case but they differ in the BWR case. A likely explanation for the higher observed count rates is that the neutron source strengths may have been underestimated. The different trends predicted for the BWR assembly may be the result of enrichment zoning.

Analysis of the photon response shows predictions to be about 50% above the measured values when using one set of flux-to-dose-rate conversion factors. One possible issue is the accuracy of the flux-to-dose-rate conversion factors. Allowing for uncertainties as to threshold settings and other possible calibration issues, we feel that the agreements are reasonable and trends seem to be as predicted.

In summary, this work gives us the ability to specify an arbitrary neutron or gamma source distributed within a spent-fuel assembly and then to estimate the measured signals in a Fork detector. In a practical application, normalization factors would probably be required. But, a number of factors affecting Fork detector measurements need further investigation. In particular, it would seem worthwhile to investigate the detector performance as a function of the boron content in the cooling pool. We also discussed the effect of enrichment zoning in fuel assemblies. If the outer rods in an assembly have enrichments that are different from those of the inner rods, this factor would quite likely significantly affect the Fork detector response. The models developed here together with the two-dimensional burnup-simulation model in SCALE are well suited to address the important issue of zoning in fuel assemblies. This consideration is quite important if MOX fuel assemblies are being monitored.

12. References

1. Rinard, P.M.; Boser, G.E.; *Safeguarding LWR Spent Fuel with the Fork Detector*, LA-11096-MS; Los Alamos National Laboratory, Los Alamos, NM; March 1988.

2. *SCALE: A Modular Code System for Performing Standardized Computer Analyses for Licensing Evaluations*, ORNL/TM-2005/39, Version 5, Vols. I–III; Oak Ridge National Laboratory, Oak Ridge, TN; April 2005. Available from Radiation Safety Information Computational Center at Oak Ridge National Laboratory as CCC-725.

3. Briesmeister, J. F., ed.; *MCNP—A General Monte Carlo N-Particle Transport Code—Version 4C*, LA-13709-M; Los Alamos National Laboratory, Los Alamos, NM; April 2000.

4. Personal communication to B. D. Murphy, Oak Ridge National Laboratory, from EURATOM staff; February 2004.

5. ANS-6.1.1 Working Group, M. E. Battat (Chairman); *American National Standard Neutron and Gamma-Ray Flux-to-Dose Rate Factors,* ANSI/ANS-6.1.1-1977 (N666); American Nuclear Society, LaGrange Park, IL; 1977.

6. ICRP Committee 3 Task Group, P. Grande and M. C. O'Riordan (Chairmen); *Data for Protection against Ionizing Radiation from External Sources: Supplement to ICRP Publication 15*, ICRP-21; International Commission on Radiological Protection; Pergamon Press, Oxford; April 1971.

7. Murphy, B. D; Primm III, R. T.; "Simulation of Mixed-Oxide and Low-Enriched Uranium Fuel Burnup in a Pressurized Water Reactor and Validation against Destructive Analysis Results," *Nuclear Science and Engineering* **142,** 258-269 (2002).